Int. J. Electrochem. Sci., 8 **(2013)** 8632 - 8644

International Journal of
ELECTROCHEMICAL
SCIENCE
www.electrochemsci.org

Effects of Magnesia Content on Spinel Magnesium Ferrite Formation

N. M. Deraz[1,*] *and Omar H. Abd-Elkader*[2]

[1] Chemistry Department , College of Science, King Saud University, P.O. Box 2455, Riyadh 11451, Saudi Arabia.
[2] Electron Microscope Unit, Zoology Department, College of Science, King Saud University, Riyadh 11451, Kingdom of Saudi Arabia.
[*]E-mail: nmderaz@yahoo.com

Received: 27 April 2013 / *Accepted:* 13 May 2013 / *Published:* 1 June 2013

The goal of this research is to prepare magnesium ferrite spinel solid solution with magnesia-rich composition, $MgFe_2O_4$. (*n-1*)MgO, in one step by simple method. The structural and morphology properties of the resulting materials were determined by XRD, SEM and EDX techniques. The as prepared samples show the formation of sponge-like materials. The XRD measurements showed that the as synthesized samples consisted entirely of well crystalline spinel magnesium ferrite, $MgFe_2O_4$, as a single phase. The presence of magnesium ferrite in excess amount of magnesia brought about formation of magnesium ferrite spinel solid solution with magnesia-rich composition. However, the excess amount of magnesia resulted in a decrease in both the degree of crystallinity and lattice constant with subsequent an increase in the density of the investigated compounds. The crystallite size was decrease as the magnesia content increases with subsequent contraction in the ferrite lattices. The gradient and homogeneity of elementary species included in $MgFe_2O_4$. (*n-1*)MgO system contains were discussed.

Keywords: XRD; SEM; EDX; MgO; $MgFe_2O_4$; Solid Solution.

1. INTRODUCTION

Magnetic ceramic materials have been attracted special attention due to chemical stability as well as high electrical resistivity. One of the most magnetic ceramics is spinel solids. Presently spinel type ferrites with general formula MFe_2O_4 have found their important applications such as those in hyperthermia, information storage systems, microwave devices, magnetic recording media, electronic industries, humidity sensors and green anode materials [1- 3]. Among spinel ferrites, magnesium

ferrite ($MgFe_2O_4$) is a soft magnetic n-type semiconducting material. In addition, $MgFe_2O_4$ belongs to the partially inverse spinel and it can be considered as a collinear ferrimagnet whose degree of inversion depends on the thermal history of the material and the preparation method [4]. Spinel magnesium ferrite possesses many attractive properties like high catalytic activity, high magnetic permeability, humidity and gas sensing characteristics. Moreover, Mg ferrite has high resistivity, high Curie temperature, and environmental stability makes it most suitable candidate for wide range of sensing applications [5, 6]. However, the cation distribution in the lattice of magnesium ferrite is sensitive to different variables such as molar ratio, thermal treatment, precursors, preparation route and doping with foreign cations….etc. Indeed, the cation distribution can be affected various properties of ferrite materials such as structural, electrical, magnetic and catalytically activity characteristics [7, 8].

The effect of metal ion substitution such as Al, Ge, Cu, Ni, Cr, Sm–Gd, Ce–Gd on the magnetic properties of $MgFe_2O_4$ has been reported in the literature [9-13]. Various Mg-Cd ferrite samples having general formula $Mg_{1-x}Cd_xFe_2O_4$ (x = 0, 0.2, 0.4, 0.6, 0.8 and 1) doped with 5% Y^{3+} were prepared by oxalate co-precipitation technique [14]. The results revealed that the doping with Y^{3+} led to a decrease in the grain size of the as prepared ferrites. The saturation magnetization, magnetic moment, remanent magnetization and coercive force increase with Cd^{2+} content up to x = 0.4 and thereafter show decreasing trend. Coercivity and saturation magnetization displays particle size dependent behavior. The reduction in the grain size as compared to un-doped samples improves the magnetic properties. The dc resistivity decreases with temperature and increases with Cd^{2+} content. These values are higher than that obtained from ceramic method [14].

A large number of methods have been developed to prepare Mg ferrite such as the standard ceramic and citrate precursor techniques [15, 16]. On the other hand, any co-precipitation process is highly pH sensitive. In addition, the sol–gel technique is more sophisticated requiring stringent drying conditions and expensive alkoxide precursors. Furthermore, any wet-chemical routes require high temperature to obtain the final product of powder with expected crystal structure [17]. Combustion process of synthesizing magnesium ferrite is one of the best approaches due to low processing time, relatively lower operating-temperature and cost effectiveness. However, combustion route for the synthesis of oxide materials imparts significant advantages like good stoichiometric control and ultrafine particle formation with narrow size distribution [7, 18 - 21].

Nano-magnetic magnesium ferrite particles were prepared by combustion method using different ratios between Mg/Fe precursors and glycine as a fuel. Significant effects of these ratios on the structural, morphological and magnetic properties of the as-synthesized nano-particles have been investigated. The results obtained revealed that the as-prepared Mg ferrite nano-particles have the nanometer size and partially inverse spinel structure. The as synthesized magnesium ferrites have various crystallite sizes ranging from 8 to 66 nm. It found that the magnetic properties of Mg ferrite nano-particles depend upon their size and crystallinity. The saturation magnetization for the sample having the highest crystallite size was 32.85emu/g [7]. The aim of the present work is to investigate influence of iron non-stoichiometry on structural and morphological properties of magnesium spinel type ferrite.

2. EXPERIMENTAL

2.1. Preparation Technique

Two samples of Fe/Mg mixed oxides were prepared by mixing different proportions of iron and magnesium nitrates with calculated amount of glycine [7]. The mixed precursors were concentrated in a porcelain crucible on a hot plate at 400 ^{o}C for quarter hour. The crystal water was gradually vaporized during heating and when a crucible temperature was reached, a great deal of foams produced and spark appeared at one corner which spread through the mass, yielding a voluminous and fluffy product in the container. In this investigation, the ratio of the glycine: magnesium: ferric nitrates were 4: (1.5 and 2): 2 for S1 and S2 samples, respectively. The chemicals employed in the present work were of analytical grade supplied by Prolabo Company.

2.2. Characterization techniques

An X-ray measurement of various mixed solids was carried out using a BRUKER D8 advance diffractometer (Germany). The patterns were run with Cu K_α radiation at 40 kV and 40 mA with scanning speed in 2θ of 2 ° min^{-1}.

The crystallite size of $MgFe_2O_4$ present in the investigated solids was based on X-ray diffraction line broadening and calculated by using Scherrer equation [22].

$$d = \frac{B\lambda}{\beta \cos\theta} \qquad (1)$$

where d is the average crystallite size of the phase under investigation, B is the Scherrer constant (0.89), λ is the wave length of X-ray beam used, β is the full-width half maximum (FWHM) of diffraction and θ is the Bragg's angle.

Scanning electron micrographs (SEM) was recorded on JEOL JAX-840A electron micro-analyzer. The samples were dispersed in ethanol and then treated ultrasonically in order to disperse individual particles over gold grids.

Energy dispersive X-ray analysis (EDX) was carried out on Hitachi S-800 electron microscope with an attached kevex Delta system. The parameters were as follows: accelerating voltage 15 kV, accumulation time 100s, window width 8 μm. The surface molar composition was determined by the Asa method, Zaf-correction, Gaussian approximation.

3. RESULTS

3.1. Identification of $MgFe_2O_4$ spinel solid solution compound

The XRD patterns for S1 and S2 samples containing of magnesium ferrite Spinel solid solution with the magnesia-rich composition are given in Fig. 1.

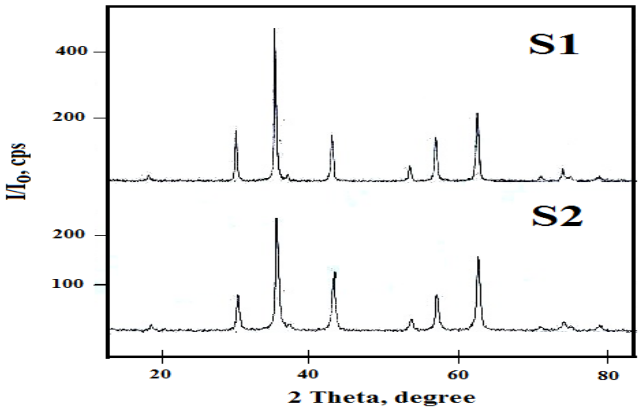

Figure 1. XRD pattern for the S1 and S2 samples.

Investigation of the previous figure revealed that: (i) The S1 and S2 samples consisted entirely of magnesium ferrite, $MgFe_2O_4$, (JCPDS card No. 17- 464) with different planes (1 1 1), (2 2 0), (3 1 1), (2 2 2), (4 0 0), (4 2 2), (5 1 1), (4 4 0), (6 2 0), (5 3 3), (4 4 4), (6 4 2) and (7 3 1) of cubic spinel structure. The absence of any second phase indicates to formation of $MgFe_2O_4$ as a singles phase. The space group of magnesium ferrite is *Fd3m* [23]. One cannot ignore the presence of amorphous magnesium oxide because the Mg/Fe ratio for the S1 and S2 samples equals to 0.43 and 0.5, respectively, while the stoichiometry for the previous ratios is 0.33. This finding confirms the presence of MgO inside the samples studied. (ii) The increase in the amount of MgO resulted in a decrease in the peaks height of magnesium ferrite. In other words, the diffraction peaks of $MgFe_2O_4$ phase for the S2 sample become less sharp than that of the S1 sample. However, intensities of the diffraction peaks for S2 sample is lower than that for S1 sample indicating to the decrease in the crystallinity of the as prepared samples by increasing the content of magnesia. This decrease reveals a decrease in the size of phase investigated.

3.2. The structural properties control of $MgFe_2O_4$ nano- powders

Table 1. Some structural parameters for the crystalline phases involved in the magnesium ferrite.

Samples	$MgFe_2O_4$			
	d (nm)	a (nm)	V (nm^3)	D_x (g/cm^3)
S1	42	0.8381	0.5887	4.5153
S2	29	0.8361	0.5845	4.5478

The control in the structural properties of $MgFe_2O_4$ nano-powders can be achieved by tuning the molar ratio of MgO to Fe_2O_3. Indeed, the increase in the magnesia content brought about a decrease in the crystallite size (d) of the as synthesized magnesium ferrite depending upon the decrease in the crystallinity of these crystallites as shown in Table 1. Also, Table 1 shows the values of the

lattice constant (a), unit cell volume (V) and X-ray density (D_x) of $MgFe_2O_4$ nano- particles depending upon the data of X-ray. Increasing the amount of Mg species brought about a decrease in the values of lattice constant and unit cell volume of Mg ferrite depending upon the ionic radii of the reacting species (Fe^{2+}=0.074 nm, Fe^{3+}=0.064nm and Mg^{2+}=0.065 nm) [24]. Opposite behavior was observed for X-ray density (D_x) of Mg ferrite.

Comparing the full-width half-maximum (FWHM) of the XRD pattern of S1 and S2 samples, it is apparent that S2 powder may have lowest crystallite size as shown in Table 2. This table displays that the values of FWHM relative to the mentioned planes for the S2 sample are greater than that for the S1 sample. This confirms the contraction of the lattices of the S2 sample with subsequent decrease in their size.

Table 2. Values of full-width half-maximum (FWHM) of the XRD pattern of S1 and S2 samples.

Planes	FWHM	
	S1	S2
220	0.165	0.435
311	0.235	0.424
400	0.153	0.400
422	0.118	0.235
440	0.082	0.318
533	0.153	0.329

3.3. Formation of nano-crystalline $MgFe_2O_4$ spinel solid solution compound

Deraz reported to prepare of magnesium ferrite nano-particles by a simple and cost-effective method using different ratios between Mg/Fe precursors and fuel. It is found that the best ratio between the fuel (glycine) and metals nitrates is 1.33 in order to obtain nano-crystalline $MgFe_2O_4$ particles [7]. In this study, we aim to prepare magnesium ferrite in magnesia – rich environment by glycine – assisted combustion method. This study is extending to effect of this environment on the formation, structural and morphological properties of magnesium ferrite.

In addition to the stoichiometric spinel phase, $MgFe_2O_4$, the structural similarities of MgO and $MgFe_2O_4$ phases noted above results in wide range of solid solutions with excess magnesia spinels, $MgFe_2O_4 \cdot (n\text{-}1)MgO$, being known. This is clearly shown from the decrease in the unit cell parameter a of the spinel phase due to increase of the Mg/Fe ratio depending upon the ionic radii of the reacting ions (Mg^{2+}, Fe^{2+} and Fe^{3+}). However, the incorporation of the excess amount of Mg^{2+} cations in the magnesium ferrite spinel phase leads to a significant shift of all the diffraction lines related to magnesium ferrite to lower angle associated with the decrease in its lattice parameter.

3.4. Cation distribution

The distribution of cations between tetrahedral, and octahedral sites included in the spinel structure are more sensitive to the change in the intensities of the (2 2 0) and (4 4 0)) planes,

respectively [25]. However, the intensities of the (5 1 1)) plane is sensitive to the change in oxygen ion parameters [25]. Indeed, the Mg^{2+} ions have preferentially occupied the octahedral site yielding inverse spinel ferrite [26]. Table 3 shows the observed change in the intensities of the previous planes.

Table 3. The intensities of some hkl planes for the as prepared magnesium ferrite.

Samples	Peak height (cps)			
	I_{220}	I_{440}	I_{511}	I_{220}/ I_{440}
S1	108	141	96	0.766
S2	96	97	54	0.990

It can be seen from this table that the intensity of (4 4 0) plane is greater than that of (2 2 0) plane indicating presence of the highest percentage of reacting cations at octahedral site. However, incorporation of Mg ions in the spinel lattice brought about a decrease in the intestines of the previous planes depending upon the smaller ionic radius of Mg ions. But the extent of decrease in the intensity of (4 4 0) plane is greater than that of (2 2 0) plane, where the percentage values of this decrease are 31.2% and 11.1 %, respectively. This finding confirms that the Mg ferrite has a partially inverse spinel structure with formation of formation of solid solution having magnesia – rich composition. Also, this observation refers to presence of the highest percentage of Mg^{2+} at the octahedral site depending upon the I_{220}/ I_{440} ratio that increase by increasing the amount of magnesia. However, these findings confirm formation of partial inverse spinel magnesium ferrite with the formula $MgFe_2O_4$ [7, 27-29]. This can be expressed as:

$$(Mg^{2+}{}_{1-\delta}\ Fe^{3+}{}_{\delta})[Mg^{2+}{}_{\delta}\ Fe^{3+}{}_{2-\delta}\ ]O_4{}^{2} \qquad (3)$$

Where δ represents the degree of inversion of cation in the cubic structure.

From the data of X-ray, the distance between the reacting ions (L_A and L_B), ionic radii (r_A, r_B) and bond lengths (A–O and B–O) on tetrahedral (A) sites and octahedral (B) sites $MgFe_2O_4$ crystallites were summarized in Table 4. This table showed that the increase in the content of magnesium resulted a decrease in the calculated values of L_A, L_B, r_A, r_B, A–O and B–O of $MgFe_2O_4$ crystallites. These findings confirm the decrease in the crystallite size, lattice constant and unit cell volume of $MgFe_2O_4$ nano- particles. These changes observed could be attributed to the increase in the Mg content which assists crystal contraction and/or the redistribution of cations among octahedral and tetrahedral sites included in the spinel structure [7].

Table 4. The values of L_A, L_B, A-O, B-O, r_A and r_B for the as prepared magnesium ferrite.

Samples	L_A (nm)	L_B (nm)	A-O (nm)	B-O (nm)	r_A (nm)	r_B (nm)
S1	0.3629	0.2963	0.2032	0.1969	0.0682	0.0582
S2	0.3620	0.2956	0.2023	0.1965	0.0631	0.0580

3.5. SEM investigation

SEM technique was used to study the morphology of the S1 and S2 samples. SEM images for the S1 and S2 samples are given in Fig. 2 A and B, respectively. These images display remarkable changes in the microstructure and porosity of the investigated system. The as prepared samples have spongy and fragile network structure with voids and pores. This observation could be attributed to the release of large amount of gases during combustion process.

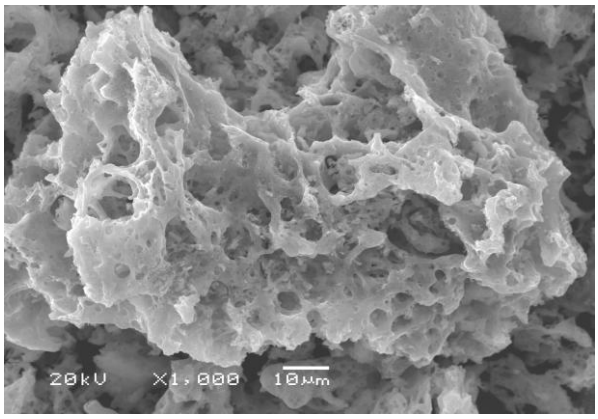

A

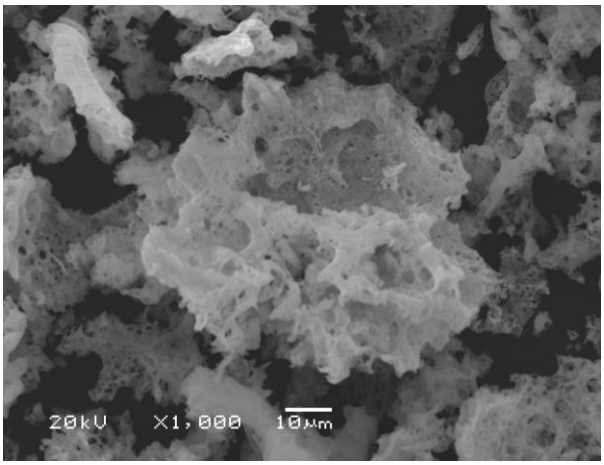

B

Figure 2. SEM images for the as prepared samples; (A) S1 and (B) S2.

3.6. EDX measurements

EDX technique was used to of the S1 and S2 samples was used to determine the effective atomic concentrations of different constituents (Mg, Fe and oxygen species) on top surface layers of the solids investigated. Fig. 3 A and B showed EDX spectrums of the previous samples at 20 keV.

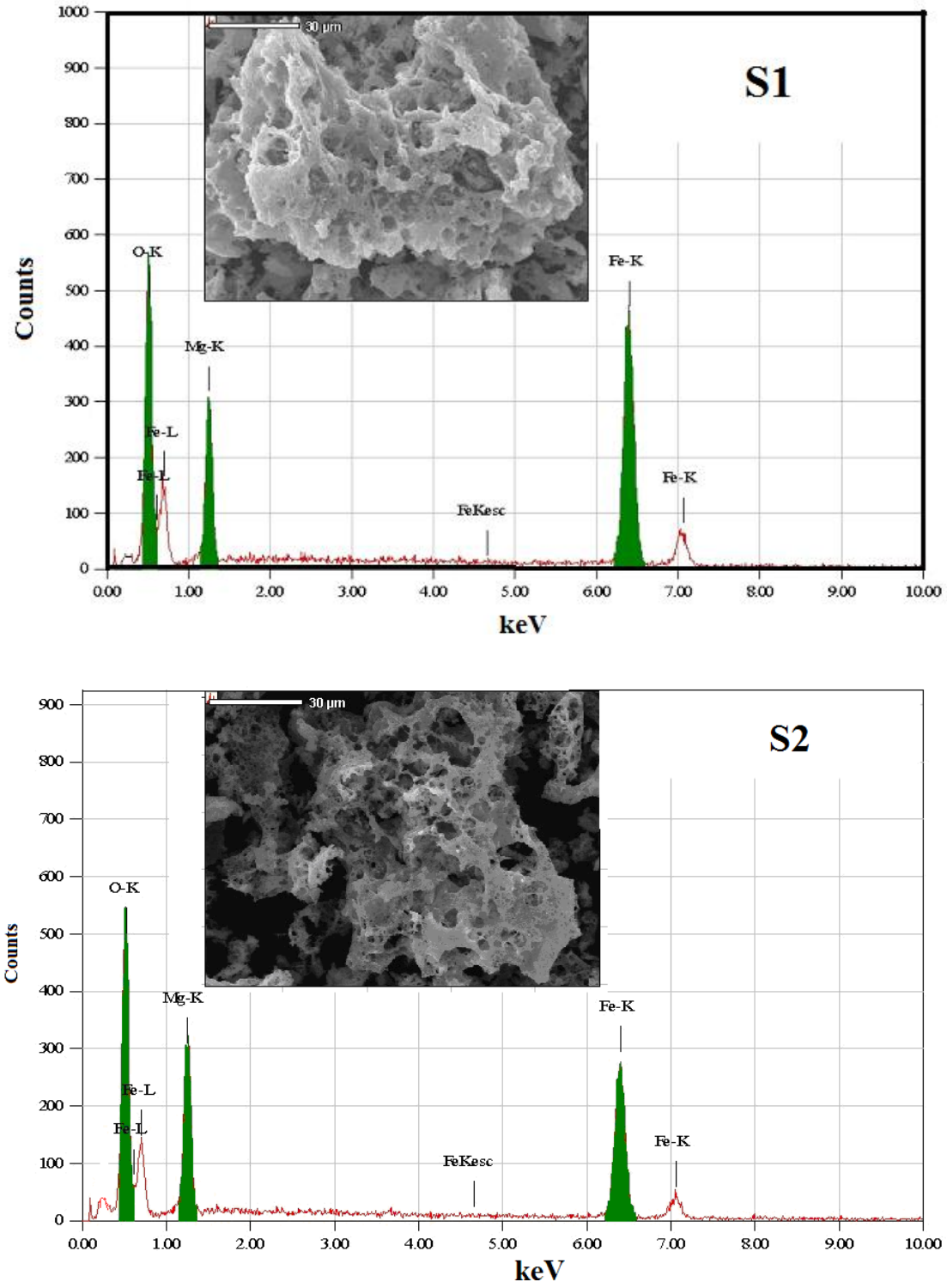

Figure 3. EDX spectrum for the as prepared samples.

Table 5 shows the relative atomic abundance of Mg, Fe and oxygen species included in the uppermost surface and bulk layers of the as synthesized. This table reveals that the surface concentrations of Mg species in the S1 and S2 samples are greater than that in the bulk of these samples. The increase in the Mg content resulted in an increase in the surface Mg/Fe ratio. However, this treatment brought about slightly change in the surface concentrations of oxygen and iron species. This indicates to formation of magnesium ferrite solid solution with magnesia- rich composition.

Table 5. The composition of the Mg/ Fe system measured by EDX technique.

Samples	Elements	Atomic abundance (%)		Surface Mg/Fe Ratio
		Calculated (Bulk)	Found (Surface)	
S1	Mg Fe O	12 56 32	18.16 54.16 27.51	0.3353
S2	Mg Fe O	12 56 32	21.29 50.29 28.42	0.4233

3.6.1. Homogeneity of elementary species in the as prepared samples

Table 6. The atomic abundance of elements measured at 20 keV and different points over the S1 and S2 samples.

Samples	Elements	Point 1	Point 2	Point 3	Point 4
S1	Mg Fe O	25.17 10.04 64.79	23.61 04.64 71.75	23.01 06.04 69.95	23.83 05.40 70.78
S2	Mg Fe O	25.92 12.63 61.46	25.60 11.52 62.89	25.93 12.69 61.37	26.50 14.66 58.84

In order to the homogeneity of elements in the as prepared samples, EDX measurements were carried over different points on the samples surface at 20 keV was carried out. The concentrations of O, Mg and Fe species included in the S1 and S2 samples are given in Tables 6. Study of this table

displays the similarity of concentrations of the elementary species at different points in both S1 and S2 samples. This confirms the homogeneity of the as prepared samples.

3.6.1. The gradient of elementary species in the as prepared samples

The elements gradient can be determined by carrying out EDX measurements at the same point on the sample surface at 5, 10, 15 and 20 keV. Thus, we can obtain the concentrations of O, Mg and Fe species from the uppermost surface to the bulk layers for the two investigated samples as shown in Tables 6 and 7.

Table 7. The atomic abundance of elements measured at different voltages over the same area for the S1 and S2 samples.

Samples	Elements	Atomic abundance (%)		
		5 keV	10 keV	15 keV
S1	Mg	39.69	26.66	24.53
	Fe	60.31	15.21	07.84
	O	00.00	58.13	67.63
S2	Mg	39.69	30.69	27.64
	Fe	60.31	29.14	18.60
	O	00.00	40.17	53.67

It can be seen that the uppermost surface layer of the two prepared samples is O- and Mg-rich layer depending upon the surface concentrations of Mg and oxygen species for the S1 and S2 samples decrease as the applied voltage increases from 5 to 20 keV. However, the absence of the Fe species at uppermost surface layer of the two prepared samples depending upon the surface concentrations of Fe species at 5 keV are zero for the S1 and S2 samples. As the applied voltage increases above the previous limit (5 keV) as the surface concentration of Fe species increases. This indicates that the concentration of Fe species at the uppermost surface layer is lower than that at the bulk of the as prepared materials. These findings suggest a possible redistribution for the elements involved in the as synthesized composites with formation of spinel magnesium ferrite solid solution with magnesia-rich composition.

4. DISCUSSION

Glycine - assisted combustion route was used for preparation of spinel magnesium ferrite [7]. Authors reported that this method is simple and low cost by using appropriate amount of glycine followed by heating at low temperature. In this study, we aim to prepare spinel magnesium ferrite solid solution with magnesia- rich composition by combustion method using a suitable amount of glycine. In

fact, XRD measurements display formation of magnesium ferrite, $MgFe_2O_4$, as a single phase. However, XRD analysis no shows any diffraction line related to any second phase such as MgO or Fe_2O_3. This indicates formation of solid solution between $MgFe_2O_4$ and MgO yielding $MgFe_2O_4$. *(n-1)*MgO system.

Various authors reported that formation of ferrite is starting by formation of small amounts of ferrite as a rigid oxide lattice at the interface of constituent oxides [7, 30-33]. The complete formation of ferrite is depending upon the diffusion or the mobility of the reacting species through the rigid layer at the interface of constituent oxides. The diffusing ions might be Mg^{2+} and Fe^{2+} including Fe^{3+} on the basis of detecting Fe^{2+} in the interface [7, 30-33]. At the ferric oxide surface, the magnesia species reacted with ferric oxide yielding magnesium ferrite, Fe^{2+} ions and oxygen gas. But at magnesia surface, the resulted Fe^{2+} ions and oxygen gas reacted with magnesia and so on. The excess magnesium oxide could be dissolved in the lattices of iron species (Fe^{3+}/Fe^{2+}) and magnesium ferrite forming spinel magnesium ferrite solid solution with magnesia- rich composition depending upon the difference in the ionic radii. The dissolution process can be can be simplified by the use of Kröger's notations [34] in the following manner:

$$2Mg^{2+} + Fe^{3+} \rightarrow 2Mg(Fe^{3+}) + C.V \qquad (2)$$

$$Mg^{2+} + Fe^{3+} \rightarrow Mg_{\Delta} + Fe^{2+} + 1/2O_2 \qquad (3)$$

$Mg(Fe^{3+})$ is the divalent magnesium ions located in the positions of host iron oxides in Fe_2O_3; Mg_{Δ} is magnesium ions located in the interstitial positions of ferric oxide lattice; C.V. created cationic vacancies. The dissolution of magnesium ions in the lattices of both iron oxide and magnesium ferrite led to creation of cationic vacancies and contraction of the ferrite lattices. These findings resulted in an increase in the mobility of cations of reacting oxides and an increase in formation of nano- sized spinel magnesium ferrite solid solution with magnesia- rich composition. In other words, the amount of MgO which can be dissolved in $MgFe_2O_4$ to give a solid solution can be regarded as the following equation:

$$n\text{MgO} + Fe_2O_3 \rightarrow MgFe_2O_4 - (n\text{-}1)\text{MgO} \qquad (4)$$

Indeed, XRD measurements revealed that the presence of excess amount of MgO during preparation of magnesium ferrite led to a decrease in the crystallite size and lattice constant and unit cell volume with subsequent increase in the X-ray density of $MgFe_2O_4$ spinel. The produced $MgFe_2O_4$ - (*n-1*)MgO system have homogeneity and gradient of the elementary species as shown in the SEM and EDX studies.

5. CONCLUSIONS

Combustion route can be used to synthesis of partially inverse spinel magnesium ferrite, $MgFe_2O_4$, solid solution with magnesia- rich composition using glycine as fuel. The presence of excess

amount of magnesia affect the structural and morphological properties of the as synthesized ferrite samples. Characterization of the as prepared $MgFe_2O_4$ - (*n-1*)MgO system were investigated by XRD, SEM and EDX techniques. The X-ray diffraction measurements confirm the formation of single phase cubic spinel structure of the samples studied. Various structural parameters of the as prepared system have been determined. The most of these parameters decrease with the increase in magnesia content. The as prepared samples have a sponge-like structure.

ACKNOWLEDGEMENT
This project was supported by King Saud University, Deanship of Scientific Research, College of Science Research Centre.

References

1. K. A. Mohammed, A. D. Al-Rawas, A. M. Gismelseed, A. Sellai, H. M. Widatallah, A. Yousif, M. E. Elzain, M. Shongwe, *Physica* B 407(2012)795.
2. P. Poddar, H. Srikanth, S.A. Morrison, E.E. Carpenter, *J. Magn. Magn. Mater*., 288 (2005) 443–451.
3. N. Kikukawa, M. Takemori, Y. Nagano, M. Sugasawa, S. Kobayashi, *J. Magn. Magn. Mater*., 284 (2004) 206.
4. V.B. Kawade, G.K. Bichile, K.M. Jadhav, *Mater. Lett*., 42 (2000) 33.
5. S.A. Oliver, R.J. Willey, H.H. Hamdeh, G. Oliveri, G. Busca, *Scr. Mater.* 33 (1995)1695.
6. G. Busca, E. Finocchio, V. Lorenzelli, M. Trombetta, S.A. Rossini, *J. Chem. Soc. Faraday Trans*. 92 (1996) 4687.
7. N.M. Deraz, A. Alarifi, *J. Analyt. Appl. Pyrolysis* 97 (2012) 55.
8. K.K. Bamzai a,n, GurbinderKour a, B.Kaur a, S.D.Kulkarni, *J. Magn. Magn. Mater.*, 327 (2013) 159.
9. K. S. Kim,S.H.Han,H.G.Kim, *Journal of the Korean Physical Society* 54(2) (2009) 886.
10. D. R. Sagar, C. Prakash, P. Kishan, *Solid State Communications* 68 (1988) 193.
11. A. Pradeep, G. Chandrasekaran, *MaterialsLetters* 60(2006)371.
12. V. K. Mittal, S. Bear, R. Nithya, M.P. Srinivasan, S. Velmurugan, S.V. Narasimhan, *J.Nucl. Mater*. 335 (2004) 302.
13. P. P. Hankare, V.T. Vader, N.M. Patil, S.D. Jadhav, U.B. Sankpal, M.R. Kadam, B.K. Chougule, N.S. Gajbhiye, *Mater. Chem. Phys*. 113 (2009) 233.
14. Ashok B. Gadkari, Tukaram J. Shinde, Promod N. Vasambekar, *Mater. Res. Bull*. 48 (2013) 476
15. M. Singh, S.P. Sud, *Mater. Sci. Eng*. B 83 (2001) 180.
16. B.S. Chauhan, R. Kumar, K.M. Jadhav, M. Singh, *J. Magn. Magn. Mater.* 283 (2005) 71.
17. Z. Yue, Ji Zhou, L. Li, H. Zhang, Z. Gui, *J. Magn. Magn. Mater*. 208 (2000) 55
18. Y. Li, J. Zhao, J. Han, X. He, *Mater. Res. Bull*. 40 (2005) 981–989.
19. N. Rezlescu, N. Iftimie, E. Rezlescu, C. Doroftei, P.D. Popa, *Sens. Actuators* B 114(2006) 427.
20. A. S. Mukasyan, P. Epstein, P. Dinka, *Proc. Combust. Inst*. 31 (2007) 1789.
21. K.C. Patil, S.T. Aruna, T. Mimani, *Curr. Opin. Solid State Mater. Sci*. 6 (2002) 507.
22. B.D. Cullity, Elements of X-ray Diffraction, Addison-Wesly Publishing Co. Inc. 1976 (Chapter 14).
23. J.A. Franco, F.C. e Silva, *Appl. Phys. Lett*. 96 (2010) 172505.
24. L. John Berchmans, R. Kalai Selvan, P.N. Selva Kumar, C.O. Augustin, *J. Magn. Magn. Mater.* 279 (2004) 103.
25. [N. M. Deraz, *Int. J. Electrochem. Sci.*, 7(2012) 4596.

26. Y. Kinemuchi, K. Ishizaka, H. Suematsu, W. Jiang, K. Yatsui, *Thin Solid Films* 407 (2002) 109.
27. H. Okawa, J. H. Lee, T. Hotta, , S. Ohara, , S.Takahashi, T. Shibahashi, Y. Yamamasu, *J. Power Sources* 131 (2004)251.
28. D.S. Mathew, R.S. Juang, *Chem. Engin. J.* 129 (2007) 51.
29. Z. Wang, Z. Lazor, P. Saxena, H. St.C O' Neill, *Mater. Res. Bull*. 37 (2002) 1589.
30. A. Azhari, M. Sharif Sh., F. Golestanifard, A. Saberi, *Mater. Chem. Physics* 124 (2010) 658.
31. J.G. Paik, M.J. Lee, S.H. Hyun, *Thermochim. Acta* 425 (2005) 131.
32. R.E. Carter, *J. Am. Ceram. Soc*. 44 (1961) 116.
33. Alper, High Temperature Oxides, Academic Press, New York, 1970.
34. F.A. KrÖger, Chemistry of Imperfect Crystals, North-Holland, Amsterdam, 1964.